ORIGINAL RESEARCH

Quantitative Short Echo Time ^{1}H-MR Spectroscopy of Untreated Pediatric Brain Tumors: Preoperative Diagnosis and Characterization

A. Panigrahy
M.D. Krieger
I. Gonzalez-Gomez
X. Liu
J.G. McComb
J.L. Finlay
M.D. Nelson, Jr.
F.H. Gilles
S. Blüml

PURPOSE: Our aims were to evaluate the metabolic profiles of pediatric brain tumors with short echo time (TE) MR spectroscopy and absolute quantitation of metabolite concentrations (in mmol/kg of tissue) and to describe metabolic features that distinguish individual tumor types and that may help to improve preoperative diagnosis of specific tumors.

METHODS: MR imaging examinations of 60 patients with untreated brain tumors (14 medulloblastomas, 5 anaplastic astrocytomas, 3 low-grade astrocytomas, 17 pilocytic astrocytomas, 4 anaplastic ependymomas, 5 ependymomas, 3 choroid plexus papillomas, 3 choroid plexus carcinomas, and 6 pineal germinomas) were reviewed. Single-voxel proton MR spectroscopy with a TE of 35 ms was performed and absolute metabolite concentrations were determined by using fully automated quantitation.

RESULTS: Taurine (Tau) was significantly elevated in medulloblastomas ($P < .00001$) compared with all other tumors pooled (All Other). Tau was also observed consistently, at lower concentration, in pineal germinomas. Creatine (Cr) was significantly reduced in pilocytic astrocytomas, distinguishing them from All Other ($P < .000001$). The MR spectra of choroid plexus papillomas exhibited low Cr ($P < .01$) concentrations; however, myoinositol was elevated ($P < .01$) and total choline (tCho) ($P < .0001$) was reduced relative to All Other. Choroid plexus carcinomas had low Cr ($P < .01$ versus All Other) and the lowest Cr/tCho ratio ($P < .0001$ versus All Other) among all tumors studied. Guanidinoacetate was reduced in low-grade astrocytomas and anaplastic astrocytomas ($P < .00001$) versus All Other, whereas ependymoma and anaplastic ependymomas exhibited particularly low *N*-acetylaspartate ($P < .00001$ versus All Other).

CONCLUSION: Quantitative proton MR spectroscopy reveals features of pediatric brain tumors that are likely to improve preoperative diagnoses.

Initial surgical resection is an important therapeutic step in the treatment of malignant brain tumors. In the future, refined methods of initial surgical approaches to treat pediatric patients with brain tumors will make accurate preoperative assessment of tumor location and extent, as well as the determination of tumor histology, more important. During the last decade, proton (^{1}H)-MR spectroscopy has been demonstrated to be valuable in the evaluation of pediatric brain tumors. Several studies have shown that MR spectroscopy can help differentiate common pediatric brain tumors.[1-10] Most studies published have used long echo times (TE) and have focused on evaluating abnormalities of *N*-acetylaspartate (NAA), total choline (tCho), and lactate (Lac) by analysis of ratios relative to creatine (Cr). These studies have shown that brain tumors in general have elevated levels of choline and reduced levels of NAA. Tumors also exhibited elevated Lac, which is believed to accumulate in necrotic areas of tumors or as a by-product of anaerobic glycolysis.

Short TE MR spectroscopy permits the observation of more metabolites, and the spectra are superior in respect to signal intensity-to-noise ratio (SNR). At the same time, fully automated postprocessing software providing robust quantitative output has become available.[11] Elevated taurine (Tau), an amino acid that has not been detected with long TE MR spectroscopy, has recently been observed independently in medulloblastoma by several groups using short TE MR spectroscopy and was found to be an important differentiator of this tumor type from other common pediatric brain tumors.[12-14]

In our study, a more comprehensive evaluation of metabolic profiles of pediatric brain tumors has been conducted by measuring absolute concentrations of all metabolites detectable with current standard methods of short TE MR spectroscopy.

The specific goals of this study were to measure absolute metabolite concentrations of common pediatric brain tumors by using short TE MR spectroscopy and to describe metabolic features that distinguish individual tumor types and that may help to improve preoperative diagnosis of specific tumors.

Materials and Methods

Patients

^{1}H-MR spectra of 77 patients studied between March 2001 and February 2005 with newly diagnosed untreated brain tumors were retro-

Received April 12, 2005; accepted after revision August 2.

From the Department of Radiology (A.P., X.L., M.D.N., S.B.), the Division of Neurosurgery (M.D.K.), the Department of Neuropathology (I.G.-G., F.H.G.), and the Childrens Center for Cancer and Blood Diseases (J.L.F.), Childrens Hospital Los Angeles, Los Angeles, Calif; and the Rudi Schulte Research Institute (S.B.), Santa Barbara, Calif.

This work was supported by grants 5R33-CA096032-03 (National Cancer Institute) and U01-CA97452-02 (National Childhood Cancer Foundation).

A portion of this work was presented at the annual meeting of the Radiological Society of North America, Chicago, Ill, November 2004.

Dr. Panigrahy received the 2006 Cornelius G. Dyke Memorial Award for this article.

Address correspondence to: Stefan Blüml, PhD, Department of Radiology, Childrens Hospital Los Angeles, MS 81, 4650 Sunset Blvd, Los Angeles, CA 90027

Table 1: Patient demographics

	WHO Grade	Subjects	S/I	No. of Spectra	Sex (F/M)	Age (mean ± SD)
Study subjects		60	27/33	78	25/35	7.22 ± 5.18
PNET (medulloblastoma)	IV	14	0/14	16	6/8	6.2 ± 3.6
Anaplastic astrocytoma	III	5	5/0	5	2/3	12.4 ± 6.5
Low-grade astrocytoma	II	3	2/1	4	2/1	5.2 ± 1.6
Pilocytic astrocytoma	I	17	6/11	21	8/9	6.2 ± 4.9
Anaplastic ependymoma	III	4	3/1	5	2/2	5.6 ± 3.3
Ependymoma	II	5	0/5	8	3/2	4.7 ± 3.4
Choroid plexus papilloma	I	3	2/1	6	0/3	9.2 ± 6.5
Choroid plexus carcinoma	IV	3	3/0	4	1/2	1.1 ± 1.4
Germinoma (pineal)	—*	6	6/0	9	1/5	14.4 ± 2.4

Note:—S indicates supratentorial; I, infratentorial; PNET, primitive neuroectodermal tumor.
*There is no WHO grade for germinoma. Germinomas sometimes come mixed with other primitive germ cell components such as endodermal sinus tumor, choriocarcinoma, immature teratoma, and mature teratoma. All germinoma cases included in this study were pure germinomas and responded well to radiation therapy.

spectively evaluated. Sixty of 77 satisfied the quality criteria defined in this article and were included in the final analysis (Table 1). MR imaging and spectroscopy studies were obtained as part of the routine work-up before surgery. Patients aged 5 years and younger were anesthetized with 100 to 200 mg/min/kg of propofol (Bedford Laboratories, Bedford, Ohio) throughout the MR imaging study. Tumors were resected within 3 days after the MR examination, and the specimens were reviewed independently by 2 neuropathologists. Final pathologic diagnoses were available for all patients, and consensus was reached in each case. The Institutional Review Board approved the review of clinical data of all patients included in this study. The requirement to obtain parental consent for this retrospective review was waived by the Institutional Review Board.

MR Spectroscopy Acquisition and Analyses

MR imaging and spectroscopy were performed with a 1.5T clinical scanner (Signa LX, GE Healthcare, Milwaukee, Wis). Standard clinical precontrast and postcontrast MR imaging was performed. Single-voxel ^{1}H spectra of the tumors were acquired before administration of contrast agent, by using a point-resolved spectroscopy sequence (PRESS) with a short TE of 35 ms, a TR of 1.5 seconds, and 128 signal-intensity averages. When the size of the lesion permitted, a second spectrum from a slightly different region of interest was obtained with the same acquisition parameters. Additional spectra with a TR of 1.5 seconds and a long TE of 144 ms were also acquired in some patients but were only qualitatively evaluated to clarify or confirm peak assignments when necessary. Total acquisition time including scanner adjustments for each spectrum was approximately 5 minutes. Sizes of the regions of interest varied from approximately 5 to 10 cm^3.

Quality Control: Partial Volume and Spectral Quality

Regions of interest were placed on the solid-appearing parts of the tumors and were carefully selected to minimize any partial volume (PV) with surrounding normal-appearing tissue. Regions of interest did not include significant blood, which could reduce spectral quality. All MR images covering the region of interest selected for MR spectroscopy were retrospectively reviewed by 2 investigators. Spectra were labeled as "Lesion" when there was no contamination by surrounding normal-appearing tissue or edema. Otherwise, spectra were labeled "PV-Lesion."

All spectra were reviewed for quality, and spectra of insufficient quality were not included in the final analyses. Spectra of poor quality were identified by an increased line width of the water resonance (a measure of the field homogeneity in the region of interest) of 3 or more SD above the mean line width of all tumor spectra. The line width of the water signal intensity is automatically measured and reported by the processing software, and this criterion, though the cutoff was empirically selected, is objective and does not introduce a bias into the data analysis.

Of the total 77 consecutive MR imaging/MR spectroscopy studies of untreated brain tumors that were analyzed, the lesions in 7 patients were too small to obtain a spectrum representative of tumor tissue and spectral quality did not meet the quality criterion in 10 patients.

Spectral Processing and Absolute Quantitation

The transfer of spectral and anatomical reference images to a workstation, processing of spectra, and determination of metabolite concentrations and concentration ratios were fully automated and did not require user interaction.

The region between 0.2 and 4.0 ppm of the spectra was processed by using the LCModel software (version 6; Stephen Provencher Inc., Oakville, Ont, Canada). This version of the LCModel has additional simulated model spectra for macromolecules and lipid resonances at 2.0, 1.7, 1.4, 1.3, and 0.9 ppm, which improve the quantitation of the metabolites.[15,16] Metabolite concentrations in mmol/kg of tissue for NAA, Cr, tCho, myo-inositol (mI), glutamate (Glu), glutamine (Gln), scyllo-inositol (sI), Tau, lactate (Lac), alanine (Ala), and guanidinoacetate (Gua) were determined. The independent determination of in vivo concentrations of Glu and Gln is compromised by the complex spectral appearances of Glu and Gln because of homonuclear coupling. Therefore, the more robust sum, [Glx] = [Glu] + [Gln], was determined as well.

The lipids and macromolecule contributions to the spectra were also analyzed. Because the number of equivalent protons per lipid molecule or macromolecule is unknown, these entities cannot be quantified in absolute concentrations, and arbitrary absolute intensities are reported. Lipids and macromolecules each have more than 1 peak that can be quantified. In this study, the combined lipid and macromolecule signals at approximately 0.9 ppm (LipMM09) and at approximately 1.3 ppm (LipMM13) are reported.

The fraction of cystic/necrotic tissue within the region of interest was measured as previously reported,[17] and all metabolite concentrations (except Lac) were then corrected for the various fractions of tumor and of necrotic/cystic fluid in the regions of interest. This correction is necessary because most metabolites (except for Lac and, to some extent, glucose and possibly lipids) are intracellular and virtually undetectable with current in vivo MR spectroscopy methods in

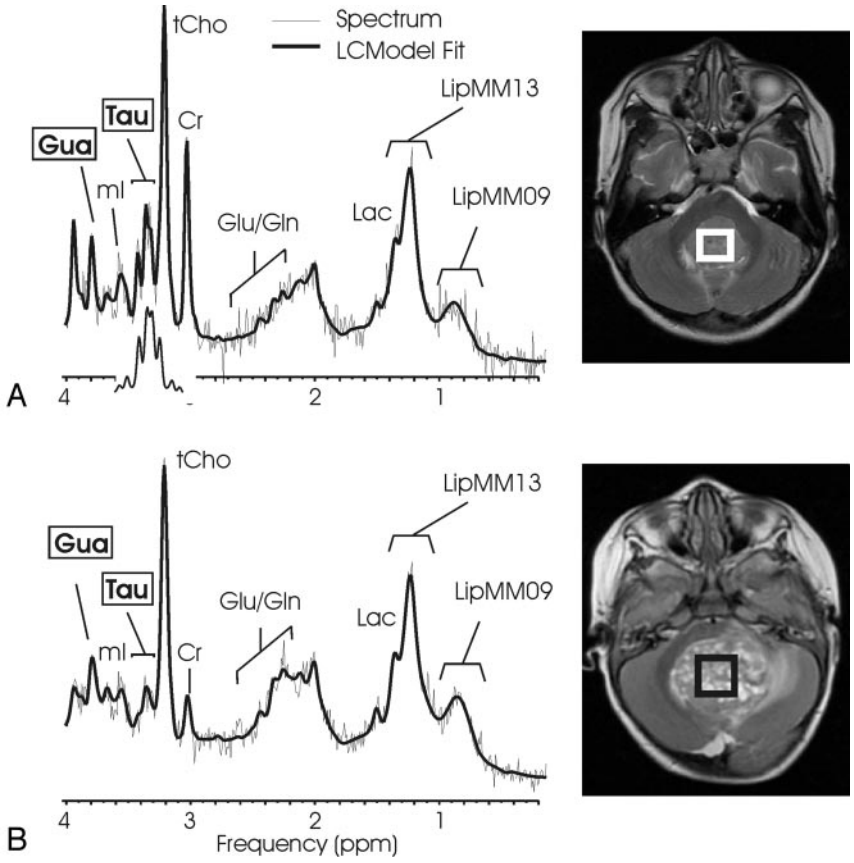

Fig 1. ^{1}H-MR spectroscopy of medulloblastoma. ^{1}H spectra of a solid-appearing medulloblastoma (*A*) and of a medulloblastoma with necrotic/cystic areas (*B*) and corresponding T2-weighted transverse fast spin-echo MR image [repetition time (TR)/echo time (TE), 3500/85 ms; 256 × 192 matrix; 2 signals acquired; echo-train length of 16; acquisition time of 2 minutes 48 seconds] indicating the region of interest. Absolute quantitation included a correction for the different fraction of cystic tissue (6% versus 48%), and spectra are scaled to allow direct comparison of peak areas. A singlet at 3.78 ppm consistent with guanidinoacetate (Gau) is observed, and taurine (Tau) is detected as a complex signal intensity at ≈3.4 ppm. Note the different levels of Tau, creatine (Cr), and glutamate/glutamine (Glu/Gln) signal intensity in the spectra. Spectra also exhibit broad lipid and macromolecule resonances at 0.9 and 1.3 ppm. One peak of the lactate (Lac) doublet at 1.33 ppm is detected as a shoulder of the broad LipMM13 resonance. *N*-acetylaspartate (NAA) is depleted, and total choline (tCho) is prominent in all spectra of medulloblastoma. The insert in spectrum A shows the spectrum of Tau scaled to the size of the fitted Tau components. Shown are the unfiltered raw data (*thin line*) and the LCModel fit to the data (*thick line*).

cerebrospinal/necrotic fluid. Omitting a correction for the fraction of CSF/necrotic fluid within the region of interest would result in an underestimation of the tissue concentrations of metabolites. For example, the signal intensities of metabolites from a voxel with 50% tissue and 50% CSF would be half of that observed from a voxel of the same dimensions but containing 100% tissue.

When more than 1 spectrum was acquired from a lesion, results from individual spectra were first averaged. Corrections for T1 and T2 relaxation of metabolites were omitted because these parameters are unknown for individual tumors and their measurement in vivo is currently not feasible within clinically acceptable total examination times.

Metabolite concentrations, both mean values and standard deviations, of standardized regions of interest in healthy controls (occipital gray matter or parietal white matter) measured with this method in this institution are consistent with data reported by other groups using similar quantitation strategies (eg, Kreis[18] and Kreis et al[19]).

Concentration Ratios

Concentration ratios relative to Cr and tCho were computed. For this study, because corrections for T1 and T2 relaxation were omitted, these ratios are directly comparable with peak area (or intensity) ratios reported in the literature. However, a correction to account for the number of equivalent protons contributing to a metabolite peak needs to be applied. For example, the tCho resonance at 3.2 ppm comprises the signal intensity from 9 equivalent protons in the choline group [-$N(CH_3)_3$], whereas the Cr peak at 3.0 ppm comprises the signal intensity from 3 protons (-CH_3). Therefore the concentration ratio [tCho]/[Cr] is one third of the peak area ratio tCho/Cr.

Statistical Analyses

Unpaired 2-tailed Student *t* tests with unequal variance were used for statistical comparisons. Tumors were subdivided into groups corresponding to their diagnostic name, and 2 sets of statistical tests were performed. In the first test, tumors of one class were compared with all other tumors pooled (All Other). Second, tumor spectra of different pathologic types were compared. There were no corrections for multiple comparisons applied. $P < .01$ was considered to indicate significance. Statistical power was >.8 for all reported *P* values. Measured concentrations and concentration ratios were tabulated as mean ± SD.

Results

Metabolic Features of Pediatric Brain Tumors

Medulloblastoma. Consistent with earlier reports,[12-14] a prominent signal intensity from Tau (Fig 1) was observed in all medulloblastoma spectra. Mean [Tau] in medulloblastoma was higher than mean [Tau] in All Other and was the most significant differentiator of medulloblastoma from All Other (Table 2). Of all tumor types studied, mean [tCho] was highest in medulloblastoma ($P < .0001$ versus All Other). However, mean [Cr], though not significant, was higher than mean [Cr] of All Other, and the [Cr]/[tCho] ratio was statistically not different from that obtained in All Other. Mean [Ala] ($P < .01$) and [Gua] ($P < .01$) were elevated compared with All Other. Note that Gua, a single peak at 3.78 ppm, overlaps only with the center resonance of 3 peaks from Gln and Glu in this region of the spectrum and can thus be separated from these 2 metabolites. Glucose (Glc) has one peak at 3.43 ppm and one at 3.80 ppm overlapping Gua. Because the Glc peak at 3.43 ppm was not elevated, the prominent signal intensity at 3.78 ppm cannot be assigned to Glc either. Among the concentration ratios evaluated, [Gln]/[tCho] ($P < .00001$), [NAA]/[tCho] ($P < .0001$), [Gln]/[Cr] ($P < .0001$), and [Glx]/[tCho] ($P < .0001$) were the most significant differentiators from All

Table 2: Absolute concentrations and concentration ratios of untreated pediatric brain tumors

	Medulloblastoma	Anaplastic Astrocytoma/ Astrocytoma	Pilocytic Astrocytoma	Anaplastic Ependymoma/ Ependymoma	Choroid Plexus Papilloma	Choroid Plexus Carcinoma	Pineal Germinoma	All Tumors
Subjects	14	8	17	9	3	3	6	60
Absolute concentrations (mmol/kg tissue)								
[NAA]	0.9 ± 0.8	2.3 ± 1.5	1.9 ± 0.8	0.2 ± 0.4****	2.4 ± 1.3	0.2 ± 0.1*****	1.3 ± 1.1	1.3 ± 1.1
[Cr]	4.7 ± 1.7	6.2 ± 2.4	1.0 ± 0.8*****	5.3 ± 3.1	1.3 ± 0.7*	1.2 ± 0.7*	3.1 ± 0.9	3.5 ± 2.6
[tCho]	5.1 ± 1.5***	3.9 ± 3.1	2.2 ± 1.1*	3.2 ± 1.5	1.8 ± 0.3***	5.1 ± 2.1	2.2 ± 0.5*	3.4 ± 2.0
[mI]	7.4 ± 4.0	12.3 ± 5.3	3.8 ± 2.1*****	13.1 ± 5.7	20.4 ± 3.7*	4.1 ± 2.0	5.2 ± 1.1*	8.2 ± 5.8
[Gln]	6.3 ± 3.5	9.51 ± 4.1	6.4 ± 3.2	8.4 ± 3.9	2.6 ± 0.6****	2.6 ± 1.5	4.4 ± 2.6	6.5 ± 3.7
[Glu]	7.5 ± 4.0	4.8 ± 2.9	3.3 ± 1.8*	2.9 ± 3.2	4.2 ± 2.4	2.7 ± 1.6	8.7 ± 2.7	5.0 ± 3.5
[Glx]†	13.8 ± 5.2	14.4 ± 4.5	9.7 ± 3.5	11.3 ± 4.4	6.8 ± 2.0	5.4 ± 0.9****	13.1 ± 3.1	11.5 ± 4.7
[Tau]	5.8 ± 2.3****	1.7 ± 1.1	0.4 ± 0.6*****	1.5 ± 1.1	0.8 ± 0.9	2.5 ± 0.6	3.0 ± 1.3	2.3 ± 2.5
[Glc]	1.0 ± 0.8	2.2 ± 1.1	2.5 ± 1.8	0.8 ± 0.7	1.6 ± 0.8	3.4 ± 2.6	0.9 ± 1.0	1.7 ± 1.5
[Lac]	3.6 ± 1.6	2.8 ± 3.9	4.3 ± 2.2	2.1 ± 2.1	0.6 ± 0.5**	1.5 ± 1.4	0.9 ± 1.6	3.0 ± 2.5
[sI]	0.2 ± 0.2	0.5 ± 0.5	0.2 ± 0.3	0.3 ± 0.3	0.9 ± 0.2	0.0 ± 0.1***	0.3 ± 0.3	0.3 ± 0.3
[Ala]	2.7 ± 1.2*	0.9 ± 0.9	1.4 ± 0.7	1.7 ± 1.0	1.0 ± 0.7	0.9 ± 1.0	2.0 ± 0.9	1.7 ± 1.1
[Gua]	3.7 ± 1.1*	1.5 ± 0.5****	2.6 ± 1.0	2.4 ± 1.0	3.0 ± 1.0	3.1 ± 0.4	3.7 ± 1.1	2.8 ± 1.2
LipMM09‡	16.7 ± 9.7	7.0 ± 2.6**	11.4 ± 5.2	14.5 ± 6.8	4.4 ± 1.6**	12.5 ± 7.5	12.0 ± 5.4	12.3 ± 7.2
LipMM13‡	64.3 ± 73.2	15.9 ± 13.4*	21.8 ± 16.1	49.6 ± 31.4	8.3 ± 2.4****	61.8 ± 73.9	63.4 ± 53.9	40.6 ± 47.9
[NAA]/[tCho]	0.2 ± 0.2***	0.9 ± 0.9	0.9 ± 0.4**	0.1 ± 0.2***	1.3 ± 0.5	0.1 ± 0.0*****	0.6 ± 0.5	0.6 ± 0.6
[Crl]/[tCho]	1.0 ± 0.4	2.1 ± 1.2	0.5 ± 0.3*****	1.8 ± 0.8	0.7 ± 0.3	0.3 ± 0.2***	1.5 ± 0.5	1.1 ± 0.8
[mI]/[tCho]	1.5 ± 0.9**	4.0 ± 2.0	1.8 ± 0.7*	4.8 ± 2.4	11.9 ± 3.7	0.9 ± 0.6*	2.5 ± 1.1	3.0 ± 2.8
[Gln]/[tCho]	1.2 ± 0.6****	2.8 ± 1.0	3.2 ± 1.7	2.9 ± 1.6	1.5 ± 0.5	0.7 ± 0.6	2.0 ± 1.2	2.3 ± 1.5
[Glu]/[tcho]	1.5 ± 0.8	1.8 ± 1.7	1.7 ± 0.9	1.3 ± 1.5	2.3 ± 1.0	0.6 ± 0.3*	4.0 ± 1.1*	1.8 ± 1.4
[Glx]/[tCho]	2.8 ± 0.9***	4.7 ± 2.2	4.8 ± 1.7	4.2 ± 2.6	3.8 ± 0.5	1.2 ± 0.7*	6.0 ± 0.8**	4.1 ± 2.0
[Tau]/[tCho]	1.2 ± 0.5**	0.3 ± 0.3	0.2 ± 0.4*	0.5 ± 0.3	0.5 ± 0.6	0.6 ± 0.3	1.4 ± 0.6	0.6 ± 0.6
[NAA]/[Cr]	0.2 ± 0.2**	0.4 ± 0.3	1.8 ± 1.2**	0.1 ± 0.1****	1.8 ± 0.4	0.1 ± 0.1***	0.4 ± 0.3*	0.7 ± 1.0
[mI]/[Cr]	1.7 ± 0.9*	2.0 ± 0.5*	3.6 ± 1.9	2.8 ± 1.4	16.6 ± 6.6	7.0 ± 7.3	1.8 ± 0.5*	3.5 ± 4.0
[Gln]/[Cr]	1.3 ± 0.7***	1.8 ± 1.0	5.5 ± 2.5***	1.7 ±0.7	2.0 ± 1.2	4.1 ± 4.0	1.3 ± 1.0	2.7 ± 2.4
[Glu]/[Cr]	1.9 ± 1.5	0.8 ± 0.5***	3.5 ± 2.5	0.8 ± 1.0*	3.1 ± 0.4	2.7 ± 1.0	2.9 ± 0.9	2.2 ± 1.8
[Glx]/[Cr]	3.3 ± 1.6	2.6 ± 1.1*	9.1 ± 4.6**	2.5 ± 1.4*	5.1 ± 1.1	7.0 ± 4.8	4.2 ± 1.1	4.9 ± 3.8
[Tau]/[Cr]	1.3 ± 0.4*	0.2 ± 0.3*	0.3 ± 0.4*	0.3 ± 0.3	0.5 ± 0.9	3.6 ± 2.8	1.2 ± 0.8	0.8 ± 1.1
[Gau]/[Cr]	0.9 ± 0.4	0.3 ± 0.1****	2.7 ± 2.3	0.6 ± 0.3*	2.4 ± 0.9	5.1 ± 4.3	1.4 ± 0.5	1.6 ± 1.9
[Glc]/[Cr]	0.2 ± 0.2*	0.4 ± 0.2	2.4 ± 1.5	0.2 ± 0.2*	1.5 ± 1.3	6.5 ± 7.9	0.3 ± 0.3	1.2 ± 2.3

Note:—*$P < .01$, **$P < .001$, ***$P < .0001$, ****$P < .00001$, *****$P < .000001$ versus All Other tumors
†[Glx] = [Glu] + [Gln].
‡Absolute intensity (arbitrary units).

Other. In addition, mean [Glc]/[Cr] was reduced ($P < .01$ versus All Other).

Pilocytic Astrocytoma. Because there was no notable difference between supratentorial (6 patients) and infratentorial (11 patients) pilocytic astrocytomas, all studies of this tumor type were pooled (Fig 2). The most significant differentiators of pilocytic astrocytoma and All Other were low [Cr] ($P < .000001$), [mI] ($P < .000001$), and [Tau] ($P < .000001$) (Table 2). Mean [tCho] was also significantly reduced ($P < .01$). Among concentration ratios, [Cr]/[tCho] was low and was the most significant differentiator of pilocytic astrocytoma from All Other ($P < .000001$). Mean [Gln]/[Cr] ($P < .0001$), [NAA]/[Cr] ($P < .001$), [NAA]/[tCho] ($P < .001$), and [Glx]/[Cr] ($P < .01$) ratios were higher than in All Other. Significantly lower than in All Other were also [mI]/[tCho] ($P < .01$), [Tau]/[tCho] ($P < .01$), and [Tau]/[Cr] ($P < .01$).

Choroid Plexus Papilloma and Choroid Plexus Carcinoma. In all 6 spectra acquired, mI was the most prominent peak in 3 patients with choroid plexus papilloma (CPP), and mean mI concentrations were highest ($P < .01$ versus All Other) in this tumor type (Fig 3, Table 2). MR spectroscopy at long TE of 144 ms confirmed the assignment of mI (insert, Fig 3*A*). Glycine, an amino acid coresonating with mI at 3.56 ppm is expected to have residual signal intensity in long TE MR spectroscopy, which was not observed. Mean [Gln] ($P < .00001$), LipMM13 ($P < .00001$), LipMM09 ($P < .001$), [tCho] ($P < .0001$), and [Cr] ($P < .01$) were lower than those measured in All Other. None of the evaluated concentration ratios were significantly different in CPP compared with All Other.

Patients with choroid plexus carcinoma (CPC) were not pooled with those with CPP because the spectra appeared to be strikingly different (Fig 3 *C*). CPC exhibited low [NAA] ($P < .000001$), [Glx] ($P < .00001$), and sI ($P < .0001$) compared with All Other. Mean [Cr] was also reduced ($P < .01$). Although the mean [tCho] of CPC was high compared with all other tumors, it did not reach significance because of the small number of patients studied. Among concentration ratios, low [NAA]/[tCho] ($P < .000001$), low [Cr]/[tCho] ($P < .0001$), and low [NAA]/[Cr] ($P < .0001$) were the most significant differentiators of CPC from All Other [mI]/[tCho] ($P < .01$), [Glu]/[tCho] ($P < .01$), and [Glx]/[tCho] ($P < .01$) were also significantly reduced.

Low-Grade Astrocytoma and Anaplastic Astrocytoma. All anaplastic astrocytomas were supratentorial, whereas 1 low-grade astrocytoma was found in the cerebellum, another

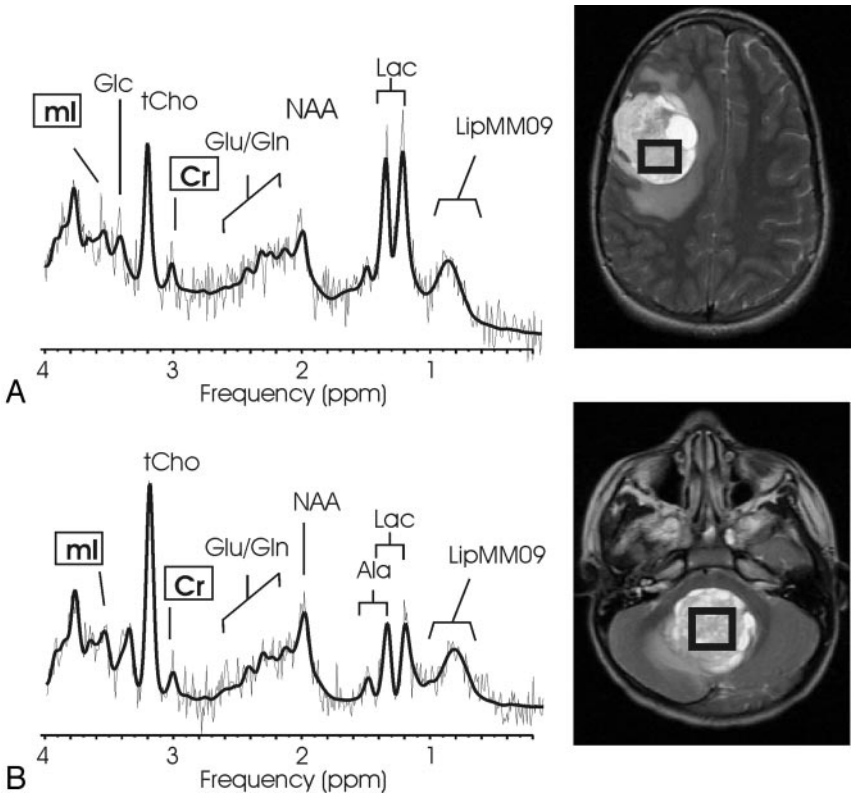

Fig 2. ^{1}H MR spectroscopy of pilocytic astrocytoma. Short echo time (TE) spectra of a supratentorial (*A*) and infratentorial (*B*) pilocytic astrocytoma and corresponding MR images indicating the regions of interest are shown. Pilocytic astrocytoma spectra are noisy because of the low cellularity of the lesions. Absolute quantitation revealed low creatine (Cr) concentrations. High lactate (Lac) and prominent total choline (tCho) and *N*-acetylaspartate (NAA) relative to creatine were noted.

was multicentric in the hypothalamic and thalamic region, and the third was located in the frontal lobe. Low-grade astrocytoma and anaplastic astrocytoma (A/AA) spectra displayed a wide range of spectral appearances. For example, in individual patients, [tCho] varied between 1.6 and 11.5 mmol/kg (Fig 4). Mean Gua concentration was lower than mean [Gua] in All Other ($P < .00001$) and was the single most significant differentiator. In addition, mean LipMM09 ($P < .001$) and LipMM13 ($P < .01$) were reduced in A/AA compared with All Other. Among concentration ratios, reduced [Gua]/[Cr] ($P < .00001$ versus All Other) was the most significant marker for all astrocytoma. Significantly reduced were also [mI]/[Cr] ($P < .01$), [Glu]/[Cr] ($P < .0001$), [Glx]/[Cr] ($P < .01$), and [Tau]/[Cr] ($P < .01$).

Ependymoma. Spectra from ependymoma and anaplastic ependymoma (E/AE) exhibited considerable heterogeneity (Fig 5). For example, in individual patients, mI concentrations ranged from 4.2 to 22.0 mmol/kg. When all studies were pooled, mean [NAA] was reduced and was the most significant differentiator between E/AE and All Other ($P < .00001$). [NAA]/[Cr] ($P < .00001$) and [NAA]/[tCho] ($P < .0001$) were also highly significantly reduced. [Glu]/[Cr] ($P < .01$), [Glx]/[Cr] ($P < .01$), [Gua]/[Cr] ($P < .01$), and [Glc]/[Cr] ($P < .01$) were also significantly reduced compared with All Other.

Pineal Germinoma. Pineal germinoma was the only tumor type other then medulloblastoma in which Tau was consistently observed (Fig 6). Both mean [tCho] ($P < .01$) and [mI] ($P < .01$) were reduced and significantly different compared with All Other. Among concentration ratios, elevated [Glx]/[tCho] ($P < .001$) was the most significant differentiator from All Other. [Glu]/[tCho] was elevated ($P < .01$) and [mI]/[Cr] was reduced ($P < .01$) for this tumor.

Presurgical Differentiation of Pairs of Tumors

A common situation is the consideration based upon MR imaging of 2 or more tumor types in the differential diagnosis. For example, a lesion may have features on MR imaging that are not specific for medulloblastoma, pilocytic astrocytoma, astrocytoma, ependymoma, or even a choroid plexus carcinoma, and a definite diagnosis cannot be rendered. Results of pair-wise comparisons of MR spectroscopic features of the different tumor types that may improve presurgical diagnoses are summarized in Table 3. Only 3 parameters per comparison are shown to keep the table compact. Medulloblastoma was best distinguished from A/AA and E/AE by elevated [Tau]/[Cr] ratio and Gua concentrations (Fig 7*A*) and from pilocytic astrocytoma by elevated [Tau] and reduced [NAA]/[tCho] ratio (Fig 7 *B*). A/AA and pilocytic astrocytoma were best separated by [Cr] and the [Cr]/[tCho] ratio (Fig 7 *C*). None of the investigated parameters individually provided a complete separation of E/AE from A/AA because of the heterogeneity of these 2 tumor types. Statistically the most significant separation was achieved by the NAA concentration and the absolute intensity of the lipid and macromolecule signal intensity at 0.9 ppm (Fig 7 *D*). E/AE and pilocytic astrocytoma were best separated by [Cr] and the [NAA]/[tCho] ratio. In addition, despite the small number of patients studied, CPP appeared to be readily distinguishable from CPC. In CPC, mean [mI] and [Glx]/[tCho] were 20% and 30% of that measured in CPP, respectively (Fig. 7 *E*).

Among patients with astrocytoma, 5 of 8 had tumors of the more malignant anaplastic astrocytoma type (WHO grade III versus WHO grade II for low-grade astrocytoma). When data from these 2 groups were compared, mean [Cr] (7.5 ± 2.1 versus 3.6 ± 1.1 mmol/kg, $P < .05$) was higher and [Glx]/[Cr] (2.0 ± 0.7 versus 2.9 ± 1.5, $P < .05$) was lower in the group with anaplastic astrocytoma.

Among patients with ependymoma, 4 of 9 had more malignant anaplastic ependymoma (WHO grade III versus WHO grade II for low-grade ependymoma). Mean was higher in low-grade ependymoma than in anaplastic ependymoma and was significantly different (16.5 ± 4.7 versus 8.8 ± 3.9 mmol/kg, $P < .05$). In addition, the mean ratios [Gln]/[Cr] (1.2 ± 0.7 versus 2.2 ± 0.2, $P < .05$) and [Glx]/[Cr] (1.5 ± 0.9 versus 3.6 ± 1.0, $P < .05$) were lower in low-grade ependymoma than in anaplastic ependymoma.

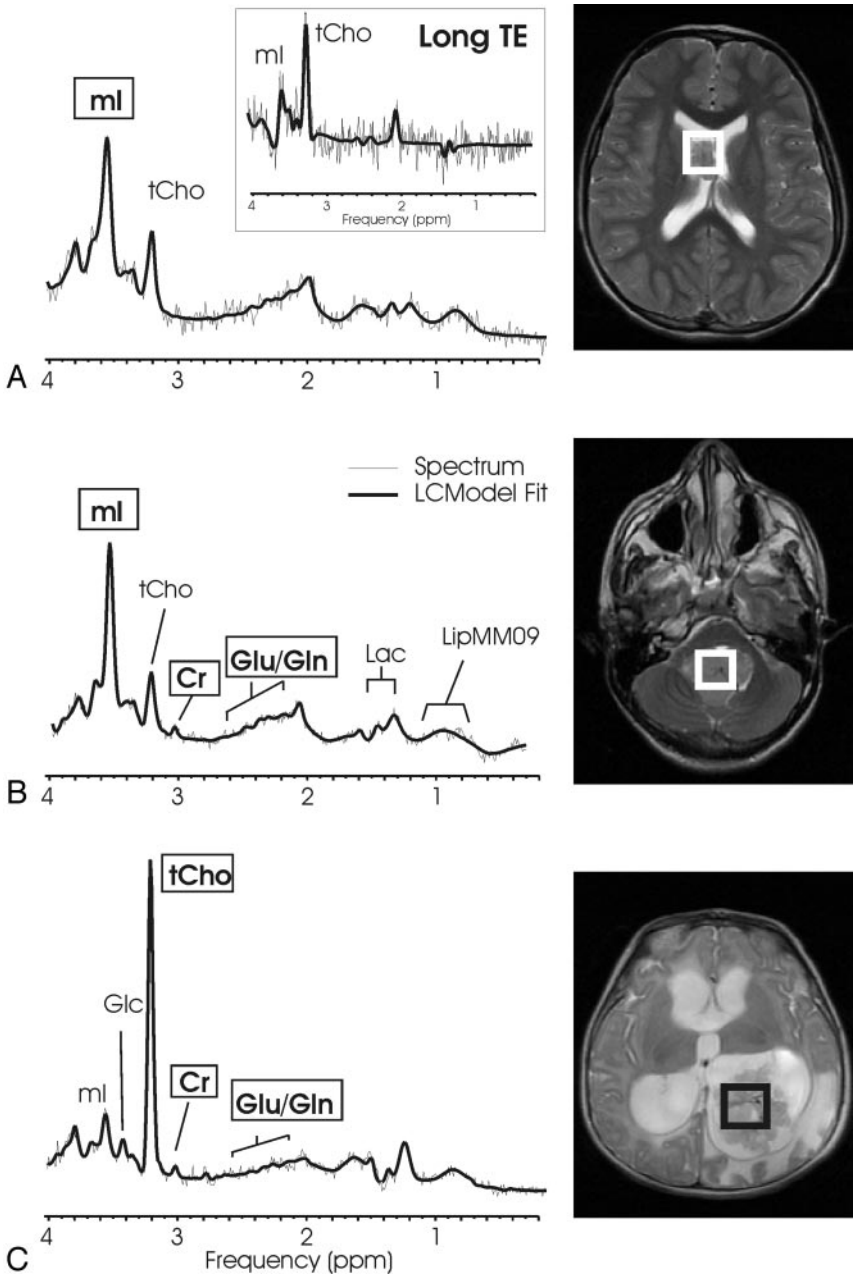

Fig 3. Choroid plexus papilloma and choroid plexus carcinoma. Short echo time (TE) MR spectra of a supratentorial (*A*) and a infratentorial (*B*) choroid plexus papilloma and of a choroid plexus carcinoma (*C*) with corresponding MR images indicating the regions of interest. Choroid plexus papilloma shows a prominent myo-inositol peak, whereas creatine (Cr) is hardly detectable. In contrast, more malignant choroid plexus carcinoma shows a prominent choline peak, whereas myo-inositol is not elevated. The insert in spectrum A displays a long TE spectrum obtained from the same region of interest. The long TE spectrum is used to rule out glycine contributing to the mI peak.

Examples for the Potential Usefulness of MR Spectroscopy

We present 3 examples demonstrating the potential usefulness of proton MR spectroscopy for presurgical diagnoses of infratentorial and supratentorial tumors.

Case 1 was a 13-year-old girl with a right frontal lobe mass. (Fig 2 *A*, Fig 7 *B*, *-C*, *-E*). There was surrounding vasogenic edema resulting in effacement of the right lateral ventricle. The mass had multiple ring-enhancing areas within the tumor after contrast administration. There was thinning of the inner table of the overlying skull. No leptomeningeal spread of the tumor was noted. The MR imaging differential included peripheral primitive neuroectodermal tumor, sarcoma, metastasis, and intrinsic glial tumor. The MR spectroscopy demonstrated a low [Cr]/[tCho] ($p = .5$) and overall low level of all metabolites consistent with a hypocellular tumor with no evidence for Tau. The absolute creatine concentration was low (0.6 mmol/kg), and MR spectroscopy was compatible with a pilocytic astrocytoma. This was confirmed after resection of the tumor.

Case 2 was a 4-year-old boy with a posterior fossa tumor (Fig 2 *B*, Fig 7 *B*, *-C*, *-E*). The scan showed a large heterogeneous mass eccentrically placed within the fourth ventricle contiguous with the cerebellum and vermis. The lesion contained multiple cysts with heterogeneous enhancement and appeared to be surrounded by larger cysts. The lesion did appear to be contiguous with a solid region of edema within the right cerebellar hemisphere and did not extend into the foramen magnum. The MR imaging differential diagnosis included medulloblastoma and ependymoma. MR spectroscopy demonstrated a low [Cr]/[tCho] ($p = .7$) and overall low level of all metabolites consistent with a hypocellular tumor with no evidence for Tau. The absolute creatine concentration was low (1.9 mmol/kg), and MR spectroscopy was compatible with a pilocytic astrocytoma. This was confirmed after resection of the tumor.

Case 3 was a 2-month-old infant (Fig 3 *C*, Fig 7 *F*). There were moderately enlarged ventricles and a multilobulated intensely enhancing mass 5 cm in diameter within the left lateral ventricle. There was no evidence of infiltration of tumor into brain tissue despite the presence of adjacent brain edema, and the MR imaging differential diagnosis included choroid plexus papilloma and choroid plexus carcinoma. MR spectroscopy did not show prominent mI, whereas tCho was striking (7.2 mmol/kg) and more than 15 standard deviations above the mean [tCho] measured in choroid plexus papilloma (1.8 ± 0.3 mmol/kg). Thus, MR spectroscopy was most consistent with a choroid plexus carcinoma and was indeed subsequently confirmed after surgical resection of the lesion.

Discussion

Pediatric brain tumors are heterogeneous with respect to their appearance on preoperative MR images, and preoperative diagnosis can be challenging. For example, although medulloblastoma tends to have low signal intensity on T2-weighted images, indicating a low-cellular tumor, there are instances in

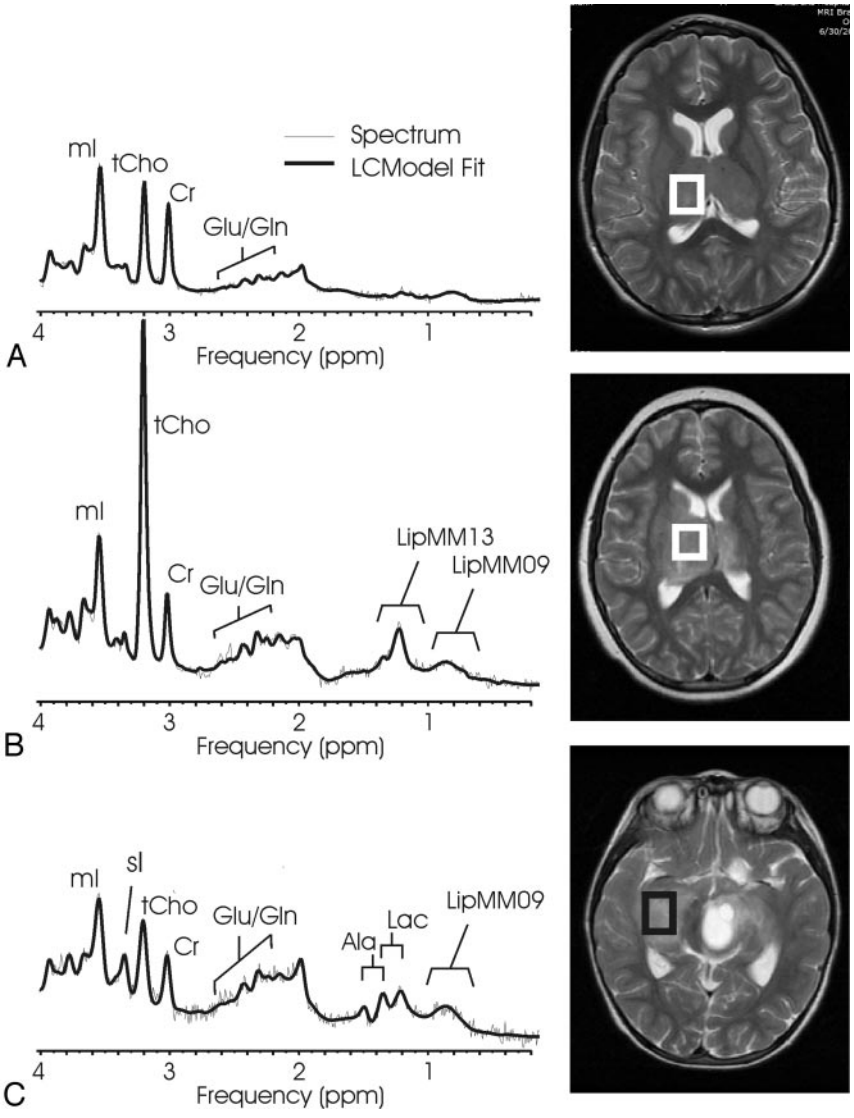

Fig 4. Low-grade astrocytoma and anaplastic astrocytoma. Short echo time (TE) MR spectra of 2 anaplastic astrocytomas (*A, -B*) and of low-grade astrocytoma (*C*) with corresponding MR images indicating the regions of interest are shown. The 3 spectra are scaled according to measured concentrations to allow direct comparison. Astrocytomas appear to be quite heterogeneous. Note the striking difference in total choline (tCho) in spectra A and B, tumors of the same diagnostic name. The prominent scyllo-inositol (sI) observed in spectrum C is not representative for all astrocytoma.

which ependymoma may present with similar features. It is common that ependymoma involves the fourth ventricular floor and extends into the foramen of Luschka. However, large medulloblastoma may have a similar growth pattern. Among pediatric brain tumors, medulloblastoma and pilocytic astrocytoma are relatively frequent. Occasionally, a cystic/necrotic medulloblastoma may have imaging characteristics that overlap posterior fossa pilocytic astrocytoma (compare with Figs 1 *B*, 2 *B*). In these situations, when MR imaging is not definitive for either of these 2 tumor types, in vivo MR spectroscopy may be valuable because the biochemical profiles of these 2 tumors are quite different.

Although short-echo quantitative MR spectroscopy may provide a means to narrow the imaging differential preoperatively, our data also showed that there is an overlap of metabolic patterns of different tumors as reported by others.[20,21] For example, ependymoma and astrocytoma are not readily distinguishable on the basis of MR spectroscopy. This feature is expected because childhood tumors are complex disease processes. Various patterns of histologic features differentiate these tumors, [22] and childhood neuroglial tumors contain histologic subsets that differ markedly in survival expectation,[23,24] reflecting the histologic heterogeneity within each diagnosis or grade.

The combination of conventional MR imaging with MR spectroscopy will result in more accurate preoperative diagnoses. A prospective study to determine the specificity of MR imaging alone versus MR imaging in combination with MR spectroscopy is currently being performed and was not a goal of this study.

Given that monitoring the course of therapy of children with brain tumors is one of the most important roles of the pediatric neuroradiologist, the accurate quantification of the preoperative metabolic fingerprint of a tumor may prove to be useful in addressing questions related to therapy, including differentiating tumor residual from postoperative change and distinguishing tumor progression from radiation necrosis. In addition, being able to fully characterize the metabolic pattern of a tumor may help predict the biologic aggressiveness of the tumor, which may alter clinical management early in the course of therapy.

Metabolites of Pediatric Brain Tumors

Total Choline (tCho). Choline is a complex peak comprising several choline-containing compounds. Mean total choline concentration in tumors was 2-fold higher than reported tCho concentration of normal brain tissue.[19,25] In a previous in vivo study by Blüml et al [26] using ^{1}H-MR spectroscopy and (phosphorous) ^{31}P-MR spectroscopy, it was found that the sum of phosphorylated cholines, phosphocholine (PCho), and glycerophosphocholine (GPC) accounts for most of the choline detected with ^{1}H-MR spectroscopy in normal tissue. This finding is consistent with in vitro analyses of the choline composition and postmortem changes in rat brain.[27] However, the composition of the choline peak in tumors is different. Both in vivo[28] and in vitro[29,30] studies demonstrated that 30%–80% of the tCho signal intensity of tumors originates from nonphosphorylated cholines. The most likely candidate is free choline, which is known to accumulate in necrotic tissue.[27,31] Of all choline-containing compounds, PCho is most associated with rapid tumor growth and malignancy.[32,33] Therefore, it is likely that the prognostic significance of tCho,

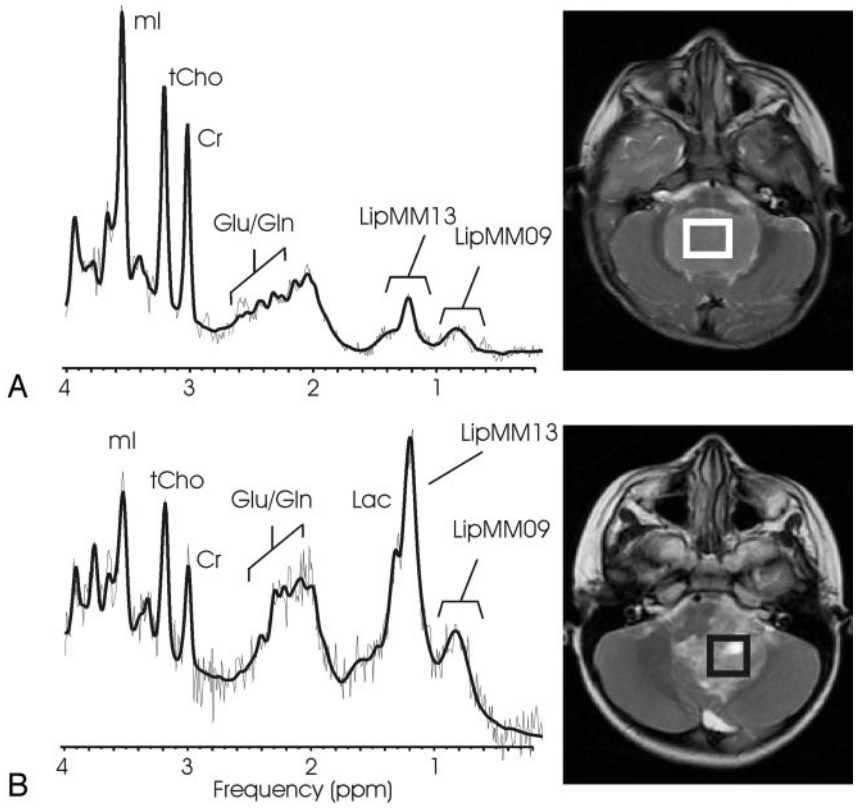

Fig 5. Low-grade ependymoma and anaplastic ependymoma. Short echo time (TE) MR spectra of a low-grade ependymoma (*A*) and of an anaplastic ependymoma (*B*) with corresponding MR images indicating the regions of interest. The 2 spectra are scaled according to measured concentration to allow direct comparison. A feature of ependymoma is very low *N*-acetylaspartate (NAA) signal intensity. In particular, no trace of NAA was found in any of the anaplastic ependymoma. Note that glutamate + glutamine (Glx) relative to creatine (Cr) is more prominent in anaplastic ependymoma.

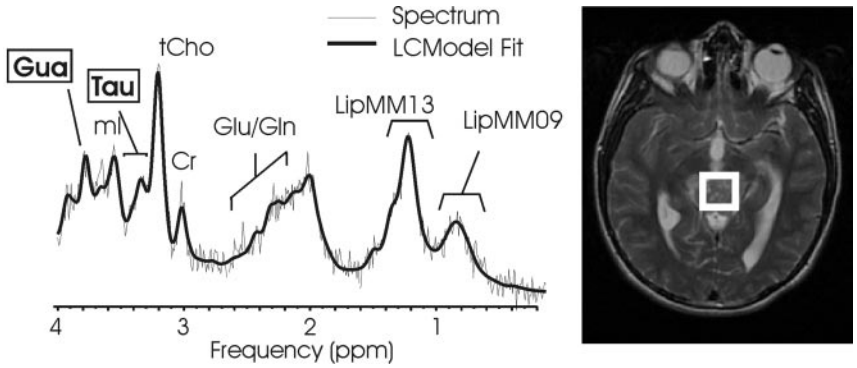

Fig 6. Pineal germinoma. Short echo time (TE) MR spectra of a pineal germinoma and MR imaging indicating the region of interest. Taurine (Tau) and guanidinoacetate (Gau) are, as in medulloblastoma, consistently observed in all pineal germinomas.

as determined with ^{1}H-MR spectroscopy, is limited. Nevertheless, tCho was particularly high in medulloblastoma (WHO grade IV) and choroid plexus carcinoma (WHO grade IV), whereas lower concentrations were measured in choroid plexus papilloma (WHO grade I) and pilocytic astrocytoma (WHO grade I). This finding is consistent with an earlier study in which absolute choline intensities, by referencing to the choline peak of control spectra acquired in the same patient with chemical shift imaging, were determined.[34] A considerable variation of tCho within tumor classes was observed. To what extent higher tCho in individual tumors is predictive of higher tumor malignancy needs to be investigated by careful long-term follow-up of patients.

Creatine (Cr) and [Cr]/[tCho]. Mean creatine of untreated tumors was approximately half of that reported in normal brain tissue,[25] consistent with in vitro studies.[35] There was no pattern of elevated or decreased Cr in more malignant tumors. Creatine concentrations are probably related to the cell type of a tumor. Particularly low [Cr] was observed in pilocytic astrocytoma and choroid plexus papilloma, but [Cr] was also low in malignant choroid plexus carcinoma as reported by Horska et al[5] in an individual patient. Because of the very low [Cr] of these tumors, [Cr]/[tCho] was tabulated instead of the more common [tCho]/[Cr], which is numerically less stable. Low [Cr]/[tCho] (or high [tCho]/[Cr]) has been associated with more malignant tumors.[36] In this study also, low-grade pilocytic astrocytoma and choroid plexus papilloma exhibited low [Cr]/[tCho] consistent with other studies.[1,2,4,5,7] Therefore, [Cr]/[tCho] is less useful than [tCho] for differentiation of high- and low-grade tumors.

N-Acetylaspartate (NAA) and [NAA]/[tCho]. NAA is present in high concentrations only in normal neurons and axons.[37,38] Tumors contain different cell types, and thus all tumors have very low or no NAA signal intensity. Therefore, any signal intensity from NAA in a tumor spectrum is unlikely to provide direct information about tumor metabolism itself but rather is an indirect marker for tumor composition by assessing the attenuation of residual neuronal/axonal cells within a lesion. Among tumors, astrocytomas, consistent with their infiltrative nature, pilocytic astrocytoma, and choroid

Table 3: Differentiation between different tumor types

	Ana. Astrocytoma/ Astrocytoma	Pilocytic Astrocytoma	Ana. Ependymoma/ Ependymoma	Choroid Plexus Papilloma	Choroid Plexus Carcioma	Pineal Germinoma
Medulloblastoma	↑ [Tau]/[Cr]***** ↑ [Tau]**** ↑ [Gua]****	↑ [Tau]**** ↓ [NAA]/[tCho]**** ↑ [Tau]/[Cr]****	↑ [Tau]/[Cr]**** ↑ [Tau]**** ↑ [Tau]/[tCho]**	↑ [tCho]**** [↑ [Lac]** ↑ [Tau]**	↑ [Glx]*** ↑ [Cr]** ↑ [Tau]**	↑ [tCho]**** ↓ [Glx]/[tCho]**** ↑ [Tau]*
Ana. Astro./Astrocytoma		↑ [Gln]/[Cr]*** ↑ [Cr]/[tCho]*** ↑ [Cr]**	↑ [NAA]* ↓ [Gua]/[Cr]* ↓ LipMM09*	↑ [Cr]** ↓ [Glu]/[Cr]** ↓ [Gln]*	↑ [Cr]** ↑ [Glx]** ↓ [Gua]*	↓ [Glu]/[Cr]* ↓ [Gua]/[Cr]* ↓ [Gua]*
Pilocytic Astrocytoma			[NAA]/[tCho]***** ↑ [NAA]***** ↑ [Gln]/[Cr]***	↑ [Lac]*** ↑ [Gln]** ↑ LipMM09**	↑ [NAA]/[tCho]***** ↑ [NAA]***** ↑ [Glx]**	↑ [Gln]/[Cr]*** ↑ [Glc]/[Cr]*** ↑ [tCho]/[Cr]**
Ana. Epend./Ependymoma				↓ [Glu]/[Cr]** ↑ [Gln]* ↑ LipMM09*	↑ [Cr]/[tCho]** ↑ [mI]* ↑ [Glx]*	↑ [Glu\/[tCho]* ↓ [Glu]/[Cr]* ↑ [mI]*
Choroid Plexus Papilloma					↑ [mI]* ↑ [tCho]* ↑ [NAA]/[Cr]*	↓ [Glx]/[tCho]* ↓ [Glx]* ↑ [NAA]/[Cr]*
Choroid Plexus Carcinoma						↓ [Glu]/[tCho]** ↓ [Glx]** ↓ [Cr]/[tCho]*

*$P < .01$, **$P < .001$, ***$P < .0001$, ****$P < .00001$, *****$P < .000001$.

plexus papilloma exhibited the highest NAA concentrations. NAA may also be detected when the region of interest comprises some of the surrounding normal tissue. In this study, this was minimized by carefully reviewing all MR images and accepting only studies in which there was no partial volume detectable. Very low NAA was detected in ependymoma; in particular, no trace of NAA was detected in all 4 cases of anaplastic ependymoma. [NAA]/[tCho] was lower in ependymoma and anaplastic ependymoma than in medulloblastoma, which is different from what has been reported by Wang et al.[1]

Myo-inositol (mI) and [mI]/[Cr]. The highest mI concentrations were measured in choroid plexus papilloma, consistent with an MR spectroscopy study of a single patient with choroid plexus papilloma reported by Tzika et al[6] In rabbit brain, the mI concentration in choroid plexus tissue was approximately one third of that measured in the cortex.[39] It has been suggested that the transport of inositol into the central nervous system might be regulated by a transporter and that the locus of that system may be, in part, in the choroid plexus.[39] It can be speculated that the accumulation of mI in choroid plexus papilloma is caused by a limited ability of cancerous tissue to facilitate the further transport of mI to other parts of the brain. Choroid plexus carcinoma did not present with a particularly high mI, and it is speculated that the relatively more mutated choroid plexus carcinoma cells have less efficient uptake of mI. The high mI concentration of astrocytoma is consistent with the idea that mI is a marker for astrocytes.[40] In this study, high mI was also observed in ependymoma and was particularly high in low-grade ependymoma. As for astrocytoma, a considerable variation of mI in individual cases was observed. Pilocytic astrocytomas, which are biologically and histologically different from other astrocytomas, exhibited low mI. In an earlier study, it was reported that higher [mI]/[Cr] is suggestive of lower grade gliomas in adults.[41] We have found no significant difference between [mI]/[Cr] in low-grade astrocytoma versus anaplastic astrocytoma or ependymoma versus anaplastic ependymoma.

Glutamate (Glu), Glutamine (Gln), and Total Glutamate + Glutamine (Glx). Glu and Gln are important components of the ^{1}H spectrum. In this study, the individual concentrations of glutamate and glutamine, as well as the more robust total concentration of glutamate plus glutamine (= Glx), were analyzed. Glu and Gln form complex and partially overlapping resonances in ^{1}H spectra, and the independent quantitation of these chemicals is challenging. Because the LCModel fits all resonances of metabolites to the spectrum simultaneously, it has increased accuracy over methods in which individual peaks are analyzed. When analyzing the covariance matrix elements of Glu and Gln, it was noticed that Glu and Gln can be reasonably well separated, though there was still considerable covariance. In general, the reliability of separation decreases with decreasing quality of spectra. For that reason, spectra of poor quality were excluded to minimize contamination of data by quantitation errors.

The highest glutamine concentrations were measured in astrocytoma and ependymoma. Among tumors, choroid plexus papilloma and carcinoma had comparably low concentration of glutamine. The highest glutamate concentrations were measured in pineal germinoma and in medulloblastoma. Medulloblastoma, pineal germinoma, and astrocytoma had mean [Glx] concentrations above the mean of all tumors, whereas [Glx] was low in choroid plexus papilloma and carcinoma. Although the role and significance of the different levels of Glu and Gln in tumor groups or individual patients is unclear, the quantitation of these metabolites proved to be useful for the separation of, for example, medulloblastoma or astrocytoma from choroid plexus papilloma.

Taurine (Tau). Tau concentrations were highest in medulloblastoma, and prominent Tau may be an important differentiator of medulloblastoma from other tumors of the poste-

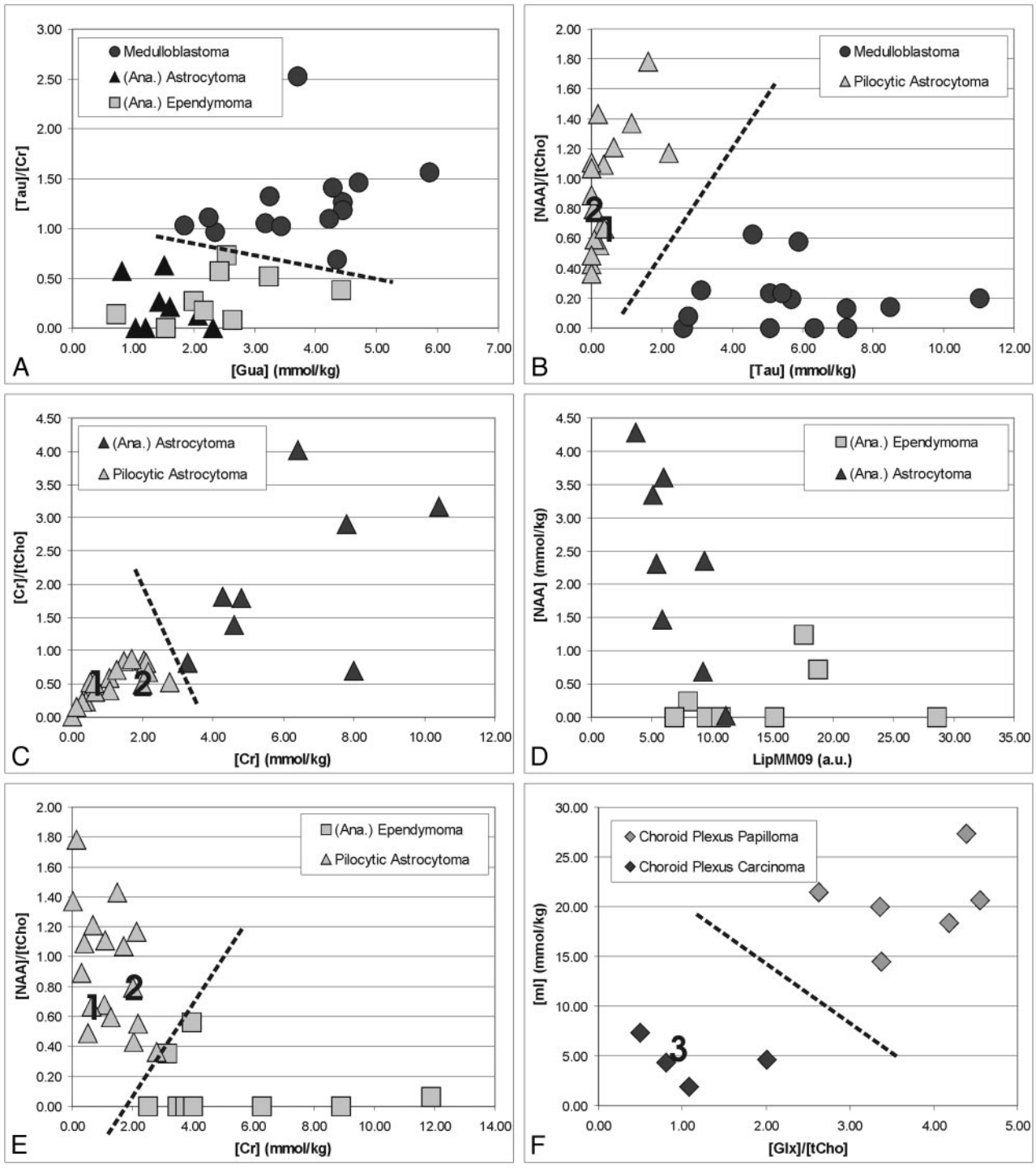

Fig 7. Differentiation of common pediatric brain tumors by quantitative ^{1}H-MR spectroscopy. Shown are measured concentrations and concentration ratios of tumors obtained from individual spectra. Labels *1*, *2*, and *3* in *B*, *C*, *E*, and *F* indicate data points obtained from individual spectra of the 3 cases presented in more detail in the Results section.

rior fossa. Elevated Tau in medulloblastoma has been independently reported by several other groups in vivo[12-14] and in vitro.[42] Tau, an aminosulfonic acid, is abundant in developing cerebellum and isocortex.[43] Tau levels are high in less-differentiated brains of neonates.[19] Elevated Tau has been described in high-grade versus low-grade astrocytoma, and it has been speculated that increased Tau is associated with increasing malignancy.[35] Tau levels were particularly low in low-grade pilocytic astrocytoma and in choroid plexus papilloma.

Glucose (Glc). Glc is the principal fuel for cells. It is broken down in a 2-step process: glycolysis with the end product pyruvate and then complete oxidation in the tricarboxylic acid (TCA) cycle. In malignant tumors, with insufficient oxygen supply, anaerobic glycolysis is believed to be increased relative to aerobic TCA-cycle activity (Pasteur effect[44,45]), and excess pyruvate is converted to Lac. It can therefore be speculated that tissue concentrations of Glc are low in malignant lesions, in which Glc is rapidly used to facilitate cell division and tumor

growth. In this limited series of patients, there was no obvious correlation of [Glc] with WHO grade or diagnosis. Medulloblastoma indeed had low Glc concentrations. However, the highest Glc concentrations were measured in choroid plexus carcinoma, a highly malignant tumor.

Lactate (Lac). Lac is an important metabolite and can be detected at pathologically elevated concentrations. High Lac is predicted for tumors on the basis of the Pasteur effect, which would also predict that tumors are acidic. However, in vivo ^{31}P-MR spectroscopy of untreated pediatric tumors demonstrated that even medulloblastomas are pH neutral or slightly alkaline.[28] The Lac level of normal CSF is significantly higher than that of tissue,[46] and Lac can accumulate in necrotic tissue. Tumor regions of interest often include, because of the nature of tumors, a significant portion of necrotic tissue. On histologic examination, some tumors also show micronecrosis that is not obvious on MR imaging. Therefore, Lac signal intensity in tumor spectra needs to be interpreted very carefully, considering the different possibilities of its origin. In this study, Lac was detected in all tumor types. The lowest Lac levels were observed in low-grade choroid plexus papilloma and in pineal germinoma. Lac was particularly high in pilocytic astrocytoma, possibly stemming from cystic regions included in the regions of interest. Lac was also prominent in malignant medulloblastoma.

Scylloinositol (sI). The sI peak at 3.36 ppm is partially overlapping with Tau. In contrast to Tau, which has a complex pattern, sI is a singlet arising from 6 equivalent protons of this molecule. The sI peak is usually very weak and thus often cannot be reliably quantified in individual spectra. In tumors, mean sI concentrations were lowest of all metabolites evaluated in this study. Only in some individual spectra was a reliable quantitation of sI possible.

Alanine (Ala). As for Lac, Ala can be observed with current methods only at pathologically elevated concentrations. Ala forms a characteristic doublet similar to that of Lac at 1.48 ppm. Ala has been previously detected in meningiomas.[21,47] In this study, Ala was also observed in other tumors consistent with in vitro studies of tissue samples in which Ala in medulloblastoma and astrocytoma was higher than that in control tissue.[42] The highest mean Ala concentrations were observed in medulloblastoma. Ala can be synthesized from and catabolized to pyruvate, which can directly enter the TCA cycle.

Guanidinoacetate (Gua). Gua is used in the liver to synthesize creatine, which is then transported to brain and muscle. A prominent peak from Gua, a singlet at 3.78 ppm, has been reported in patients with Gua methyltransferase deficiency (GAMT, EC 2.1.1.2).[48] A single peak at 3.78 ppm consistent with Gua was observed repeatedly in tumor spectra in this study and was thus tentatively assigned as Gua. Among tumors, medulloblastoma and pineal germinoma had the highest Gua concentrations. The significance of high/low Gua in individual tumor types is unclear. Nevertheless, particularly low concentrations were observed in A/AA, and Gua was the most significant differentiator of A/AA and All Other.

Lipids and Macromolecules (LipMM). The protons of the methyl groups (-CH_3) of lipid molecules resonate at 0.9 ppm, whereas protons of the methylene groups (-CH_2-) resonate at 1.3 ppm in the ^{1}H spectrum. Both resonances are broad and may comprise contributions from other macromolecules. The inclusion of LipMM resonances in the analysis significantly improves the quantitation of Lac and Ala.[16] A prominent lipid signal intensity has been observed in high-grade tumors in adults,[49] and the quantitation of lipid and LipMM signal intensity, though only in arbitrary institutional units, is of potential importance. The lipid signal intensity is believed to originate from mobile lipid molecules as a result of tissue degradation and necrosis. In this study, there was no correlation between LipMM and tumor grade. Prominent LipMM resonances were observed in some, but not all, spectra of malignant medulloblastoma and choroid plexus carcinoma. However, high LipMM intensities were also measured in less aggressive pineal germinoma responding well to chemotherapy. The intensity of the LipMM resonances in these classes exhibited considerable heterogeneity, manifested by large SDs. The lowest LipMM intensities were measured in astrocytoma and in choroid plexus papilloma. The observation of low LipMM in astrocytoma particularly may be useful to differentiate this tumor from other tumors. In contrast to an earlier study of adult astrocytoma,[50] there was no difference between low-grade astrocytoma and more malignant anaplastic astrocytoma with respect to the intensity of the LipMM levels.

Methodological Approach and Quality Control

Despite evidence for the value of MR spectroscopy to improve presurgical diagnoses, in clinical practice, the application of MR spectroscopy has been hampered by its technically challenging nature. MR spectroscopy is sensitive to artifacts and processing, and interpretation is complex and requires expert knowledge. For MR spectroscopy to be used in practice, standardized acquisition and processing methods need to be used, easy to follow rules for quality-control applied, and results presented and documented in a timely fashion to have an impact on clinical decision-making. This study was designed to overcome most of the previously mentioned obstacles, with special attention paid to fully automated processing and quantitation.

Single-voxel acquisition mode was selected over chemical shift imaging (CSI). This ensures that the quality of individual tumor spectra would not be affected adversely by unavoidable compromises accompanying CSI acquisitions from larger volumes, in which good homogeneity of the magnet field and water suppression are not always achieved uniformly. Using a short TE ensured high SNR of spectra and minimized signal intensity loss of fast-decaying peaks of metabolites such as mI, Glu, and Gln.

Because the first study goal was to describe the biochemical profile of various tumors, all studies needed to be reviewed to avoid 2 pitfalls: (1) Spectra with partial volume of surrounding normal-appearing tissue may dilute the specificity of the biochemical measurement by averaging the spectral profiles of normal tissue and tumor tissue, and (2) the quantitation of metabolites, in particular those with a complex pattern and significant overlap, is compromised or impossible in spectra of low quality. Spectra with partial volume of surrounding normal-appearing tissue were identified by visual inspection of all MR images. Spectra from regions of interest that appeared to contain edema were also excluded. This evaluation was the only subjective step in the analysis, whereas all other processing steps were fully automated and were not subject to opera-

tor bias. For example, the criterion to remove spectra of poor quality was a line width 3 SDs above the mean line width of tumor spectra. This criterion, though objective, may bias against specific tumors that are more likely to produce spectra of low quality because of inherent features such as calcification, blood (iron) deposition, or proximity to/inclusion of bone/air/tissue transitions. In 2 of 16 patients with medulloblastoma, 3 of 8 with ependymoma, 3 of 3 with nonpineal germinoma, and 2 of 19 with pilocytic astrocytoma, spectra did not reach the quality criterion.

A work-up of histologic features and correlation with MR spectroscopy results are required to determine the cause for poor quality spectra in each case. This task was outside the scope of this study. Low SNR was not a reason to discard spectra because low SNR is a feature of spectra acquired from tumors with low cellularity.[51] For example, spectra of pilocytic astrocytoma generally had lower SNR than spectra of more cellular regular astrocytoma. Patient movement was not a significant problem because many of the patients were sedated, and only in 1 patient was a repeat study required to obtain a spectrum of good quality. The fact that MR spectra that could be evaluated were obtained from only 78% of the patients is an important overall limitation of MR spectroscopy. The number of patients excluded on the basis of insufficient partial volume of tumor tissue within the region of interest could be reduced to some extent by decreasing the size of the region of interest. However, to avoid a loss of SNR, the scan time would need to be increased to obtain spectra of suitable quality.

Limitations

Absolute concentrations were determined without corrections for T1 saturation and T2 relaxation. However, these correction factors are likely to be very small, and the omissions have no impact on the interpretation of the data obtained in this study. It is well known that tumor tissue is heterogeneous with cells of different degrees of malignancy or even different histologic types in different areas of the tumor. We have acquired spectra that are representative of the mean metabolite concentration averaged over all cells contained in the region of interest. This may result in an underestimation of the metabolic heterogeneity of tumors within the same histologic class and may decrease the specificity of MR spectroscopy for differentiation of tumor types. This study does not include all brain tumors found in children. Not included in this study were tumors detected in less than 3 patients or in which final pathology was not available (eg, brain stem tumors not subject to biopsy/surgical treatment). We therefore cannot rule out the possibility that patterns described here for a particular tumor type may overlap with patterns of tumors not yet studied sufficiently.

Conclusion

In this study, concentrations of all metabolites currently detectable with routine short TE MR spectroscopy were determined and evaluated in respect to their discriminatory power between a single tumor type and All Other tumors and between pairs of tumor types. Absolute concentrations and concentration ratios of the prominent metabolites of the ^{1}H-MR spectrum (NAA, Cr, tCho, mI) provided important diagnostic information. However, less prominent spectral features, such as elevated Tau in medulloblastoma or reduced Gau in astrocytoma, also proved to be relevant for the discrimination of different tumors. As MR spectroscopy techniques further improve, more features of MR spectra can be quantified reliably and MR spectroscopy will be a powerful tool for preoperative diagnoses and for characterization of tumor metabolism in individual patients.

Acknowledgments

We thank Jane Tavare, MS, for help with statistical analyses; MR technologist Gena A. Nicholson, CRT, ARRT, for help with scanning patients; and Nilesh Ghugre, MS, for assisting with the analysis of the data.

References

1. Wang Z, Sutton LN, Cnaan A, et al. **Proton MR spectroscopy of pediatric cerebellar tumors.** *AJNR Am J Neuroradiol* 1995;16:1821–33
2. Sutton LN, Wang Z, Gusnard D, et al. **Proton magnetic resonance spectroscopy of pediatric brain tumors.** *Neurosurgery* 1992;31:195–202
3. Lazareff JA, Bockhorst KH, Curran J, et al. **Pediatric low-grade gliomas: prognosis with proton magnetic resonance spectroscopic imaging.** *Neurosurgery* 1998;43:809–17
4. Lazareff JA, Olmstead C, Bockhorst KH, et al. **Proton magnetic resonance spectroscopic imaging of pediatric low-grade astrocytomas.** *Childs Nerv Syst* 1996; 12:130–35
5. Horska A, Ulug AM, Melhem ER, et al. **Proton magnetic resonance spectroscopy of choroid plexus tumors in children.** *J Magn Reson Imaging* 2001;14: 78–82
6. Tzika AA, Vigneron DB, Dunn RS, et al. **Intracranial tumors in children: small single-voxel proton MR spectroscopy using short- and long-echo sequences.** *Neuroradiology* 1996;38:254–63
7. Hwang JH, Egnaczyk GF, Ballard E, et al. **Proton MR spectroscopic characteristics of pediatric pilocytic astrocytomas.** *AJNR Am J Neuroradiol* 1998;19: 535–40
8. Girard N, Wang ZJ, Erbetta A, et al. **Prognostic value of proton MR spectroscopy of cerebral hemisphere tumors in children.** *Neuroradiology* 1998;40: 121–25
9. Arle JE, Morriss C, Wang ZJ, et al. **Prediction of posterior fossa tumor type in children by means of magnetic resonance image properties, spectroscopy, and neural networks.** *J Neurosurg* 1997;86:755–61
10. Dezortova M, Hajek M, Cap F, et al. **Comparison of MR spectroscopy and MR imaging with contrast agent in children with cerebral astrocytomas.** *Childs Nerv Syst* 1999;15:408–12
11. Provencher SW. **Estimation of metabolite concentrations from localized in vivo proton NMR spectra.** *Magn Reson Med* 1993;30:672–79
12. Moreno-Torres A, Martinez-Perez I, Baquero M, et al. **Taurine detection by proton magnetic resonance spectroscopy in medulloblastoma: contribution to noninvasive differential diagnosis with cerebellar astrocytoma.** *Neurosurgery* 2004;55:824–29
13. Wilke M, Eidenschink A, Muller-Weihrich S, et al. **MR diffusion imaging and 1H spectroscopy in a child with medulloblastoma: a case report.** *Acta Radiol* 2001;42:39–42
14. Tong Z, Yamaki T, Harada K, et al. **In vivo quantification of the metabolites in normal brain and brain tumors by proton MR spectroscopy using water as an internal standard.** *Magn Reson Imaging* 2004;22:1017–24
15. Seeger U, Klose U, Mader I, et al. **Parameterized evaluation of macromolecules and lipids in proton MR spectroscopy of brain diseases.** *Magn Reson Med* 2003; 49:19–28
16. Auer DP, Gossl C, Schirmer T, et al. **Improved analysis of 1H-MR spectra in the presence of mobile lipids.** *Magn Reson Med* 2001;46:615–18
17. Ernst T, Kreis R, Ross BD. **Absolute quantitation of water and metabolites in the human brain. I. Compartments and water.** *J Magn Reson* 1993;102:1–8
18. Kreis R. **Quantitative localized 1H MR spectroscopy for clinical use.** *Prog NMR Spectroscopy* 1997;31:155–95
19. Kreis R, Hofmann L, Kuhlmann B, et al. **Brain metabolite composition during early human brain development as measured by quantitative in vivo 1H magnetic resonance spectroscopy.** *Magn Reson Med* 2002;48:949–58
20. Negendank WG, Sauter R, Brown TR, et al. **Proton magnetic resonance spectroscopy in patients with glial tumors: a multicenter study.** *J Neurosurg* 1996; 84:449–58
21. Howe FA, Barton SJ, Cudlip SA, et al. **Metabolic profiles of human brain tumors using quantitative in vivo 1H magnetic resonance spectroscopy.** *Magn Reson Med* 2003;49:223–32

22. Yates AJ, Becker LE, Sachs LA. **Brain tumors in childhood.** *Childs Brain* 1975; 5:31–39
23. Brown WD, Gilles FH, Tavare CJ, et al. **Prognostic limitations of the Daumas-Duport grading scheme in childhood supratentorial astroglial tumors.** *J Neuropathol Exp Neurol* 1998;57:1035–40
24. Gilles FH, Brown WD, Leviton A, et al. **Limitations of the World Health Organization classification of childhood supratentorial astrocytic tumors: Children Brain Tumor Consortium.** *Cancer* 2000;88:1477–83
25. Kreis R, Ernst T, Ross B. **Absolute quantitation of water and metabolites in the human brain. II. Metabolite concentrations.** *J Magn Reson* 1993;102:9–19
26. Blüml S, Seymour KJ, Ross BD. **Developmental changes in choline- and ethanolamine-containing compounds measured with proton-decoupled (31)P MRS in in vivo human brain.** *Magn Reson Med* 1999;42:643–54
27. Jope RS, Jenden DJ. **Choline and phospholipid metabolism and the synthesis of acetylcholine in rat brain.** *J Neurosci Res* 1979;4:69–82
28. Albers MJ, Krieger MD, Gonzalez-Gomez I, et al. **Proton-decoupled (31)P MRS in untreated pediatric brain tumors.** *Magn Reson Med* 2005;53:22–29
29. Sabatier J, Gilard V, Malet-Martino M, et al. **Characterization of choline compounds with in vitro 1H magnetic resonance spectroscopy for the discrimination of primary brain tumors.** *Invest Radiol* 1999;34:230–35
30. Usenius JP, Vainis P, Hernesmiemi J, et al. **Choline-containing compounds in human astrocytomas studied by 1H NMR spectroscopy in vivo and in vitro.** *J Neurochem* 1994;63:1538–43
31. Miller BL. **A review of chemical issues in 1H NMR spectroscopy: *N*-acetyl-L-aspartate, creatine and choline.** *NMR Biomed* 1991;4:47–52
32. Podo F. **Tumor phospholipid metabolism.** *NMR Biomed* 1999;12:413–39
33. Ramirez de Molina A, Rodriguez-Gonzalez A, Gutierrez R, et al. **Overexpression of choline kinase is a frequent feature in human tumor-derived cell lines and in lung, prostate, and colorectal human cancers.** *Biochem Biophys Res Commun* 2002;296:580–83
34. Astrakas LG, Zurakowski D, Tzika AA, et al. **Noninvasive magnetic resonance spectroscopic imaging biomarkers to predict the clinical grade of pediatric brain tumors.** *Clin Cancer Res* 2004;10:8220–28
35. Peeling J, Sutherland G. **High-resolution 1H NMR spectroscopy studies of extracts of human cerebral neoplasms.** *Magn Reson Med* 1992;24:123–26
36. Negendank WG. **Studies of human tumors by MRS: a review.** *NMR Biomed* 1992;5:303–24
37. Tallan HH. **Studies on the distribution of *N*-acetyl-L-aspartic acid in brain.** *J Biol Chem* 1957;224:41–45
38. Baslow MH. **Functions of *N*-acetyl-L-aspartate and *N*-acetyl-L-aspartylglutamate in the vertebrate brain: role in glial cell-specific signaling.** *J Neurochem* 2000;75:453–59
39. Spector R, Lorenzo AV. **Myo-inositol transport in the central nervous system.** *Am J Physiol* 1975;228:1510–18
40. Isaacks RE, Bender AS, Kim CY, et al. **Osmotic regulation of myo-inositol uptake in primary astrocyte cultures.** *Neurochem Res* 1994;19:331–38
41. Castillo M, Smith JK, Kwock L. **Correlation of myo-inositol levels and grading of cerebral astrocytomas.** *AJNR Am J Neuroradiol* 2000;21:1645–49
42. Sutton LN, Wehrli SL, Gennarelli L, et al. **High-resolution 1H-magnetic resonance spectroscopy of pediatric posterior fossa tumors in vitro.** *J Neurosurg* 1994;81:443–48
43. Flint AC, Liu X, Kriegstein AR. **Nonsynaptic glycine receptor activation during early neocortical development.** *Neuron* 1998;20:43–53
44. Pasteur L. **Experiences et vues nouvelles sur la nature des fermentations.** *Comp Rend Acad Sci* 1861;52:1260–64
45. Krebs HA. **The Pasteur effect and the relations between respiration and fermentation.** *Essays Biochem* 1972;8:1–34
46. Lentner C. *Geigy Scientific Tables.* Vol. 1. Basel, Switzerland: Ciba-Geigy; 1981: 173
47. Gill SS, Thomas DG, Van Bruggen N, et al. **Proton MR spectroscopy of intracranial tumours: in vivo and in vitro studies.** *J Comput Assist Tomogr* 1990;14: 497–504
48. Ensenauer R, Thiel T, Schwab KO, et al. **Guanidinoacetate methyltransferase deficiency: differences of creatine uptake in human brain and muscle.** *Mol Genet Metab* 2004;82:208–13
49. Negendank W, Sauter R. **Intratumoral lipids in 1H MRS in vivo in brain tumors: experience of the Siemens cooperative clinical trial.** *Anticancer Res* 1996;16:1533–38
50. Preul MC, Caramanos Z, Collins DL, et al. **Accurate, noninvasive diagnosis of human brain tumors by using proton magnetic resonance spectroscopy.** *Nat Med* 1996;2:323–25
51. Gupta RK, Cloughesy TF, Sinha U, et al. **Relationships between choline magnetic resonance spectroscopy, apparent diffusion coefficient and quantitative histopathology in human glioma.** *J Neurooncol* 2000;50:215–26